

Landslides (2009) 6:61–68
 DOI 10.1007/s10346-008-0139-y
 Received: 27 March 2008
 Accepted: 10 August 2008
 Published online: 2 September 2008
 © Springer-Verlag 2008

Bao-jun Wang · Ke Li · Bin Shi · Guang-qing Wei

Test on application of distributed fiber optic sensing technique into soil slope monitoring

Abstract Brillouin optical time-domain reflectometer (BOTDR), a newly developed distributed fiber optic sensing technique, has been proved to be a very suitable and useful technique for monitoring and early warning of structural engineering by laboratory tests and practical projects due to its unique functions, such as distributing, long distance, anti-electromagnetic interference, waterproof, etc. However, its application to geotechnical engineering, especially soil-slope engineering, has been less carried out due to the complexity of the characteristics of geotechnical materials in the field. In this paper, BOTDR technique is applied to monitor the deformation of a laboratory soil-slope model in small scale in order to test the feasibility and early-warning characteristics of this technique with monitoring the deformation of soil slope. Different types of optical fibers are planted directly in the soil-slope model or bonded to geotextiles and geogrids that are planted in the fillings of the test model. Strain measurements of the model slope under various loads are obtained by BOTDR. By data processing and analysis, the abnormal strains can be obtained distributively, and the position of the abnormal strains can be located as well. The results show much valuable information for applications of BOTDR technique into soil-slope engineering. The test proves that the BOTDR technique can be used to ensure the stability of artificial soil slope and is useful for monitoring and early warning of the artificial soil-slope engineering.

Keywords Slope deformation · BOTDR · Distributed fiber optic monitoring · Slope reinforcement

Introduction

With the economic development and the infrastructure constructing, more and more artificial slopes are encountered in practical engineering, such as embankment, road excavation, dike, surface mining, and so on. Of course, different kinds of countermeasures, such as geosynthetics, including geogrids and geotextiles, had been widely performed to ensure the stability of these artificial slopes (Lee and Manjunath 2000; Yoo 2001; Blatz and Bathurst 2001). However, due to its complexity, these artificial slopes should be real-time monitored to ensure the stability, even after the well-designed countermeasures had been carried out. At present, the monitoring techniques for slope engineering are changing from conventional point-mode monitoring to distributed and automated one with high precision and long distance (Li et al. 2003; Yin et al. 2004). The conventional-sensing technologies, such as vibrating wire sensor and strain gauge, have some disadvantages such as poor anti-interference, poor durability, and poor stability, etc., which could not meet the monitoring requirements of modern geotechnical engineering (Shi et al. 2007).

In recent years, a new technique for distributed strain sensing used for concrete structures has been developed using Brillouin

scattering based on Brillouin optical time-domain reflectometer (BOTDR; Zhang et al. 2004; Bastianini 2005). There are many unique functions of this technique, such as nondestructive capability in distributed monitoring and long-distance monitoring, anti-electromagnetic interference, waterproof, corrosion resistance, durability, etc. It is proved to be very suitable and useful for the monitoring and early warning of concrete structural engineering as well. In addition, for the small size and light weight of optical fiber, it can be easily installed into or on the surface of the monitored objects, and the optical fiber and the monitored objects are well matched in both strain and temperature changes. In concrete structure, the fiber can be installed into objects directly or installed into some steel medium before being installed into concrete structure. By some mathematical model, the monitoring data can reflect the deformation of the concrete structure. By now, BOTDR technique have been successfully applied to many concrete structure, such as tunnels, bridges, concrete piles, pipeline, rock slope, and so on (Chang and Kim 2002; Bao et al. 2007).

However, if the fiber sensors are bonded to a steel medium and then are planted with the medium into soil filling to monitor the deformation of the soil mass, the soft soil mass will slide along the steel medium when the shearing stress between steel medium, and the soil is greater than the soil shearing strength limit, which causes the monitoring data not reflect the deformation of the soil authentically. Moreover, the fragile fiber would be easily broken if the fiber sensors are directly planted into soil mass because of nonuniform settlement of the soil mass. So, it is much more complex for distributed fiber optic monitoring technique to be applied to soil-slope engineering than being applied to concrete structural engineering.

In this paper, laboratory tests are carried out in a small-scale model slope. Different types of fiber sensors are planted directly into soils or bonded to geotextiles and geogrids and then be planted into the model slope. The deformations (micro strains) of soil mass under different loads were obtained by BOTDR. The result shows that BOTDR technique can be used to monitor deformation characteristics of soil slope, and the abnormal strain can be located by analyzing the monitor data as well, which will be very helpful for early warning of soil-slope engineering. The results also show that the fibers bonded to the geogrids and geotextiles can express the deformation of the reinforcing geosynthetics, and the directly planted fibers can express abnormal strain of soil mass.

Principle of BOTDR

The detection principle of BOTDR has been fully described in above references, and only a brief description is given here.

Brillouin scattered light is caused by nonlinear interaction between the incident light and phonons that are thermally excited within the light propagation medium. This scattered light is shifted

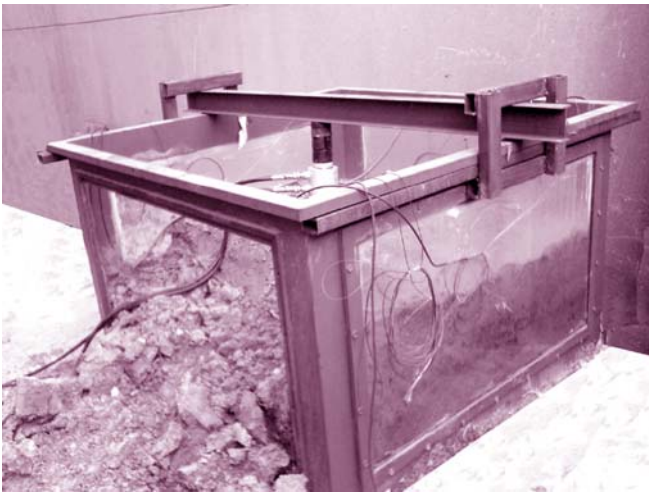


Fig. 1 Slope simulator stand

in frequency by a Brillouin shift and propagates in the opposite direction relative to the incident light. It has been found that there is a linear relationship between the strain or temperature and the frequency shift within the sensing optic fiber.

The core technique of BOTDR is Brillouin spectroscopy and OTDR that enables BOTDR to measure strain generated in optical fibers as distributing in the longitudinal direction. When the strain occurs in the longitudinal direction of optical fiber, the backscattered light of Brillouin undergoes a frequency shift that is in proportional to the strain (Horiguchi et al. 1989). Brillouin frequency shift has function of strain ε and can be expressed by Eq. 1:

$$\varepsilon = C_s(\nu_B - \nu_{B0}) + \varepsilon_0 \quad (1)$$

Where ε is the strain of optical fiber, C_s is the strain coefficient of Brillouin frequency shift, ν_B is the Brillouin frequency shift of optical fiber, ν_{B0} and ε_0 is initial Brillouin frequency shift and initial strain of optical fiber, respectively.

Brillouin frequency shift is not only the function of strain but also a function of temperature and can be expressed by Eq. 2:

$$T = C_T(\nu_B - \nu_{B0}) + T_0 \quad (2)$$

Where T is temperature of optical fiber, C_T is the temperature coefficient of Brillouin frequency shift, T_0 is initial temperature of optical fiber.

For the feature of Brillouin frequency shift being function of temperature, it is very useful to monitor the environment temperature in some special fields such as leakage of oil pipe. But in this test, the effect of temperature should be eliminated by setting temperature sensor together with strain sensor, which will be introduced in next section.

The pulse light is launched into one end of an optical fiber, and the Brillouin backscattered light occurs along the fiber and is detected at the same end. The distance (Z) from the launched end of the optical fiber is given by the Eq. 3:

$$Z = cT/(2n) \quad (3)$$

Where c is velocity of light in a vacuum, n is the index of refraction of an optical fiber, and T is the time interval between launching pulse light and receiving the scattered light. Z value can be used to locate the strain position along the optical fiber sensor.

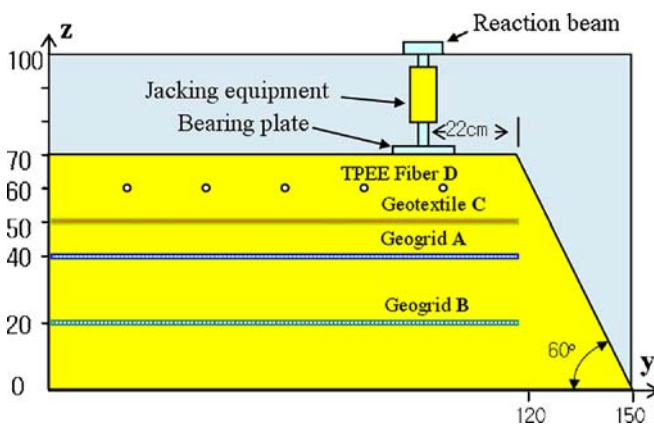


Fig. 2 Side view of fiber sensor distribution

Fig. 3 Structure of optic fiber sensors

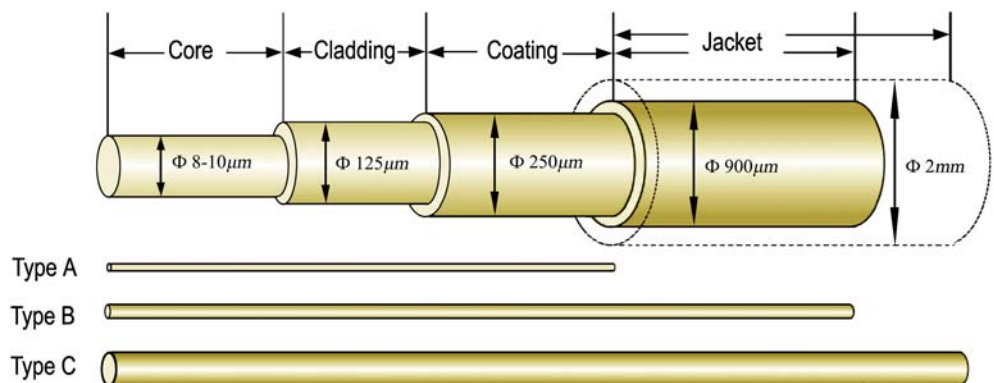


Table 1 Composition and parameters of the fiber sensors

Code	Protection and character	Diameter (mm)	Young's modulus (GPA)	Stiffness coefficient ($\times 10^6$ N/m)
Type A	Coating, tight-buffered	0.25	21.8	5.5
Type B	Nylon Jacket, tight-buffered	0.9	1.9	1.7
Type C	JPEE Jacket, tight-buffered	2.0	0.3	0.6
Type D	Nylon Jacket, loose-buffered	0.9	1.9	1.7

BOTDR AQ8603 developed by NTT Company was used in this project. It is capable of measuring the strain value at any points distributed along the optical fiber only from one end of the sensing fiber continuously and simultaneously. The measured strain range is $\pm 1.5\%$, and the measured length reaches 80 km. The measurement accuracy is up to $\pm 0.003\%$, and distance resolution is 1 m.

Slope model test

Slope simulator stand

The slope simulator stand, which is 1.5 m in width, 1.5 m in length, and 1.0 m in height, is composed of steel frame. Around the four sides, there are four transparent glass plates, and a steel plate is placed on the bottom. The glass plates of the four sides are detachable, and there is a weep hole on the bottom. There is a reaction provider made of steel on the top of the stand, and the pressure is provided by a hydraulic jack that can provide a maximum load of 500 kN between the steel structure and the surface of the slope model. Figure 1 shows the slope simulator stand.

Xiashu soil, a widely distributed soil in Nanjing, China, is selected as the filling of the model slope. This soil has an initial water content of 18.6%, cohesion of 57 kPa, and internal friction angle of 20° . The stand is filled by Xiashu soil with every 10 cm layer by layer. When the total height of the fillings is up to 70 cm, the front glass plate is removed and the slope is cut until the slope angle reached 60° . A load-bearing plate is set at the distance of 22 cm to the front edge on the surface of the slope, and the scale of load-bearing plate is 30 cm in width and 20 cm in length, as shown in Fig. 2.

Packaging of optic fiber sensor

Glass fiber used as the sensors is very fragile, and it would be broken if it were embedded directly into the monitored objects without protection. Therefore, most of optical fiber applied as distributed strain sensor consists of three parts: glass fiber (core), cladding, and coating (Ohno et al. 2002; Ding et al. 2003).

There are totally four types of fiber sensors used in this test. Two hundred micrometers optical fiber with tight-buffered coating (Type A) and 900 μm tight-buffered jacket fiber (Type B) are selected to be bonded to geosynthetics (geotextiles and geogrids).

Table 2 Performance index of short needed fabric geo-textile

Breaking strength (kN/m)	Rate of elongation (%)	CBR bursting strength (kN)	Tearing strength (kN)
8.0	40	1.2	0.2

Table 3 Performance index of glass fiber geogrid

Grid Scale (mm)	Breaking strength (kN/m)	Rate of elongation (%)	Young's modulus (GPA)
25.4 \times 25.4	50	3	67

A type of 2-mm fiber with an extra tight-buffered jacket made of TPEE (Type C) is selected to be planted in the test model directly. Compared to Type B, the TPEE jacket fiber is much more flexible and higher in strength. The structures of these three types of fiber sensors are shown in Fig. 3, and the detailed parameters are shown in Table 1.

Besides the above three types of fiber sensors, in order to eliminate the effect of temperature, a loose-buffered fiber (Type D) is also selected to monitor the strain that caused by temperature. The structure of Type D is similar with Type B, but the components, including core, cladding, and coating, can move freely inside the jacket which make the fiber sensor not affected by deformation of soil mass.

Layout of optic fiber sensor

Because geotextile and geogrid feature in light weight, high strength, and well integrity, they have been widely applied into soil-slope engineering as reinforcement material, such as embankment, dam, and so on. A type of short-needled fabric geotextile and a type of glass-fiber geogrid are selected as reinforcement materials in the test. The performance index of reinforcement materials are listed in Tables 2 and 3.

The fiber sensors, including Types A and B, is affixed by Epoxy Resin on a geotextile layer. In light of the 1-m distance resolution of BOTDR and the scale of the slope model, certain lengths of free fiber rings, which are not affixed on the geotextile and not affected by soil stress, are set at the end of each line, as shown in Fig. 4a. Five lines of fiber sensors are arranged, distance between each line is 20 cm (S) and length of each line is 1.5 m (L). In order to protect

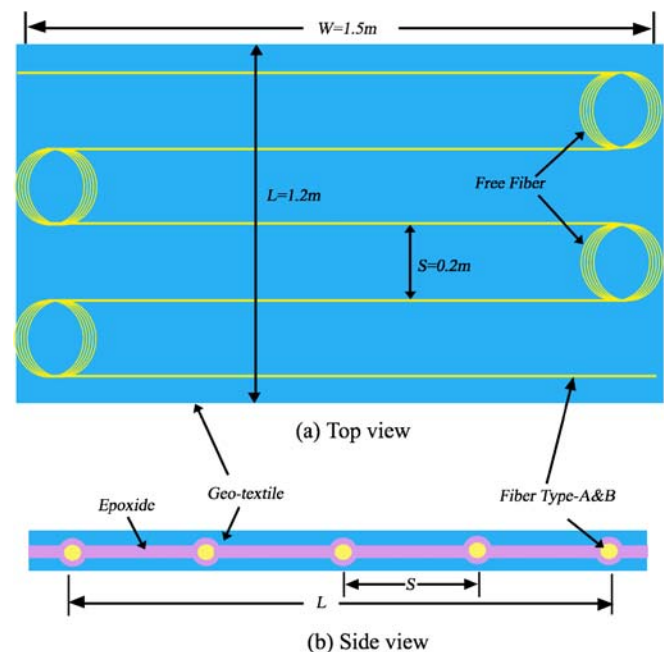


Fig. 4 Packaging of geotextile with fiber sensor

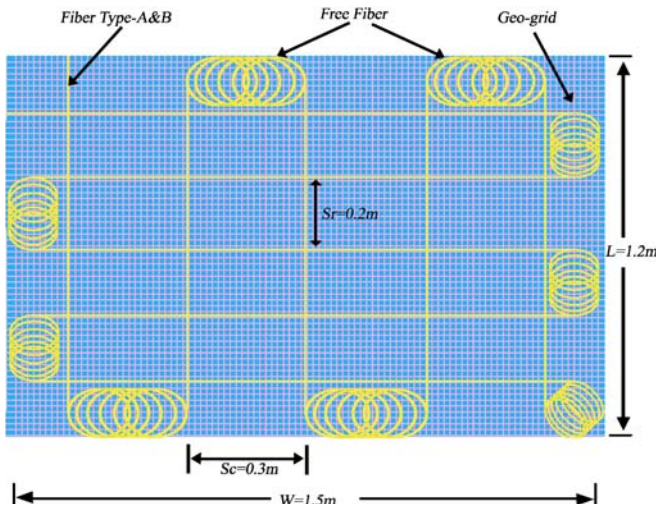


Fig. 5 Packaging of geo-grid with fiber sensor

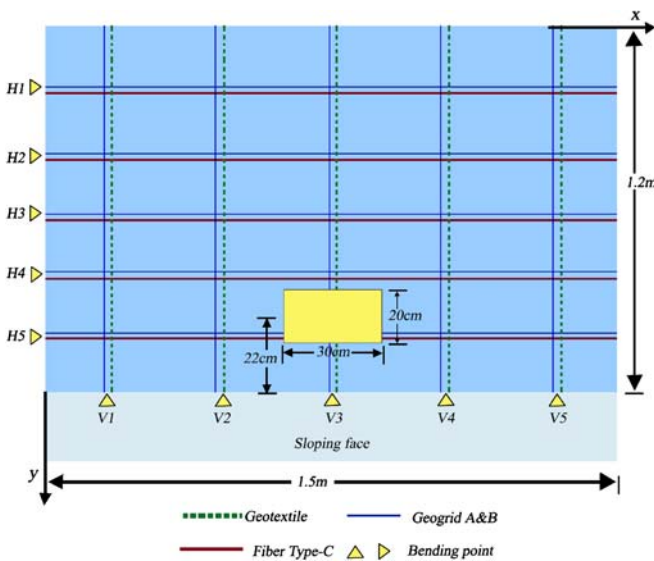


Fig. 6 Distribution and location of fiber sensor

the fiber sensor, this geotextile layer with fiber sensor is covered by another geotextile layer, as shown in Fig. 4b.

The fiber sensors Types A and B are also bonded in orthogonal grid along grids of the geogrid. Free fiber rings are also set as the alignment sensor and turn back at the end of each row and column.

The distance between each row (S_r) is 20 cm and the distance between each column (S_c) is 30 cm (see Fig. 5).

Two layers of geogrid with fiber sensors are laid at the height of 20 and 40 cm in the soil model slope, respectively. A layer of geotextile with fiber sensors is laid at the height of 50 cm of the model. Besides these two types of fiber sensors, a fiber sensor with TPEE jacket (Type C) is laid at the height of 60 cm. In order to eliminate the effect of temperature, a loose-buffered fiber is planted at the height of each above fiber sensors. The layout of these fiber sensors are shown in Fig. 2.

Locating of monitor data

All the fiber sensors described above are connected to each other and become a continuous integral fiber sensor. The monitor data obtained by BOTDR is recorded along this connected integral fiber at a designed distance (5 cm in this test). However, the maximum distance resolution of BOTDR is 1 m and certain lengths of free fibers are set along the fiber sensor, which means it is difficult to locate the accurate position of the strain only from the monitor data obtained by BOTDR. So, another OTDR is used to locate the strain position.

The measured signal for the OTDR is the Rayleigh back-scattering which is not sensitive to strain but can monitor the power loss (Christopher 2000). In the OTDR-based sensing system, the backscattered signal are captured by the OTDR to produce an attenuation profile along the fiber’s length as the function of traveling distance of the light, and so does the power loss between any two points. Thus, the OTDR can sense changes of the power loss, especially the highly localized loss, which is induced by mechanical effects such as cracking or bending. In addition to the information on fiber losses, the OTDR profiles are very useful to localize breaks, to evaluate splices and connectors, and to assess the overall quality of a fiber link generally.

In order to locate the monitor data clearly, each part of the fiber sensors is labeled as Fig. 6. After burying each layer of fiber sensors, the position of the fiber can be obtained by bending the fiber. At the bending point shown in Fig. 6, the power loss monitored by OTDR will be growing up, and the length from the bending point to the start of the integral fiber can be recorded. The distance data of each bending point to the start point of the fiber sensor is shown in Table 4.

Loading and data processing

Before loading, the initial strains are monitored by BOTDR. Pressures of 15, 20, 25, and 30 kN provided by a hydraulic jack are loaded step by step, and when the pressure is greater than 30 kN, the slope failed. The strain data are monitored by BOTDR after each loading phrase until the slope failure. The strain caused by temperature can be extracted from the data in loose-buffered fiber

Table 4 Sensor location of different parts

Code	Fiber sensor	Height(cm)	Distance from bending point to start of the integral fiber sensor (m)										
			V1	V2	V3	V4	V5	H1	H2	H3	H4	H5	
D	Fiber C	20	0.4	3.5	7.8	11.8	15.1	20.3	24.4	28.7	33.1	37.2	
C	Geotextile + fiber A & B	40	50.4	53.2	57.7	61.8	65.5	70.4	74.3	78.6	83.1	87.0	
B	Geogrid + fiber A & B	50	105.5	108.0	109.7	111.8	113.7	—	—	—	—	—	
A	Geogrid + fiber A & B	60	—	—	—	—	—	125.6	127.4	129.0	130.8	132.9	

sensor, and the soil strain caused by loading can be obtained by subtracting the initial strain and the strain caused by temperature variation. According to the location information provided by Table 4, the strain data at different locations can be obtained.

Result and analysis

The fiber sensors of Type A, including the ones emplaced in geotextile and geogrid, are all broken before loading; thus, there are no valid data obtained. The reason is that the fibers of no jacket

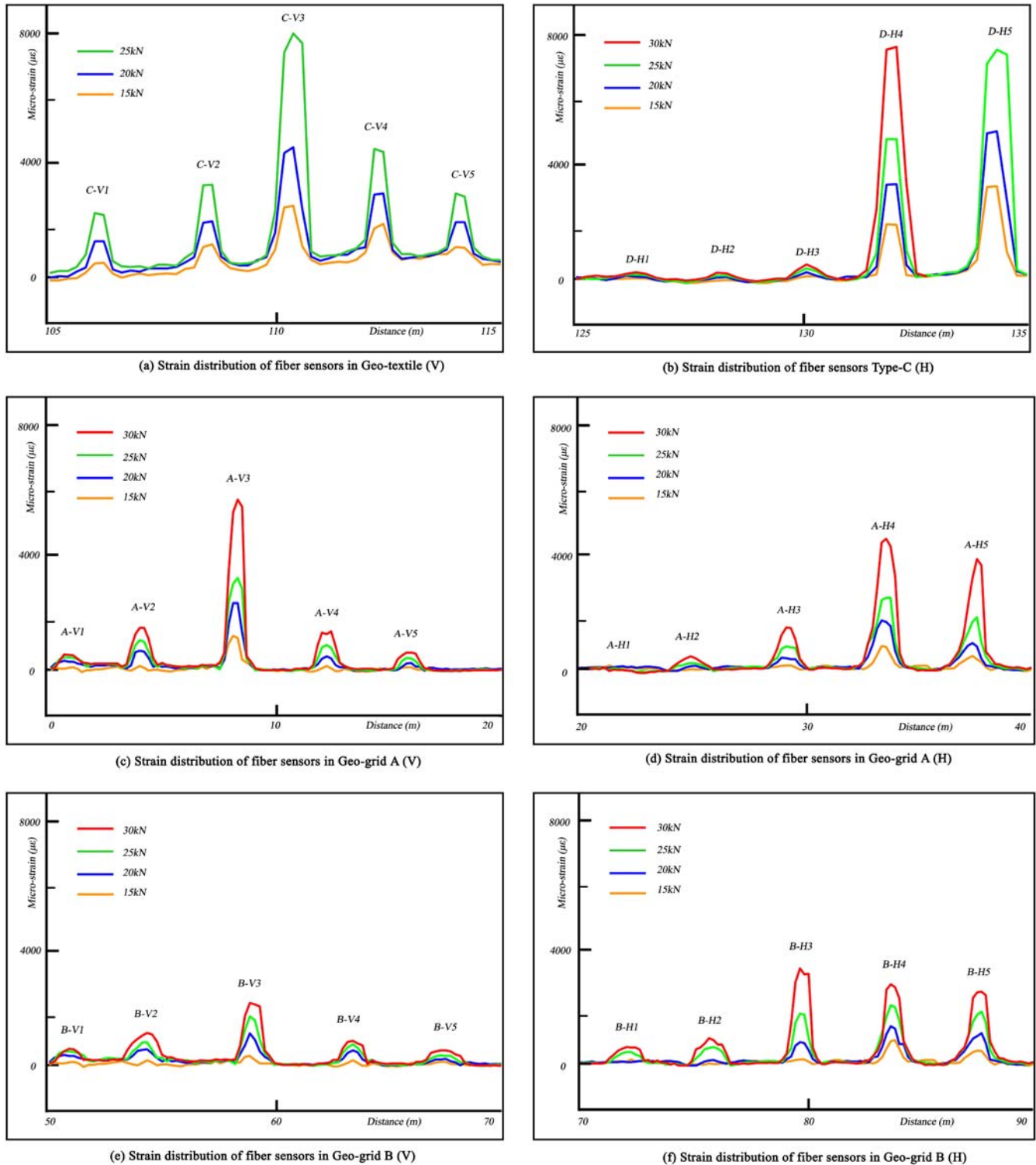


Fig. 7 Strain distribution along different parts of fiber sensors

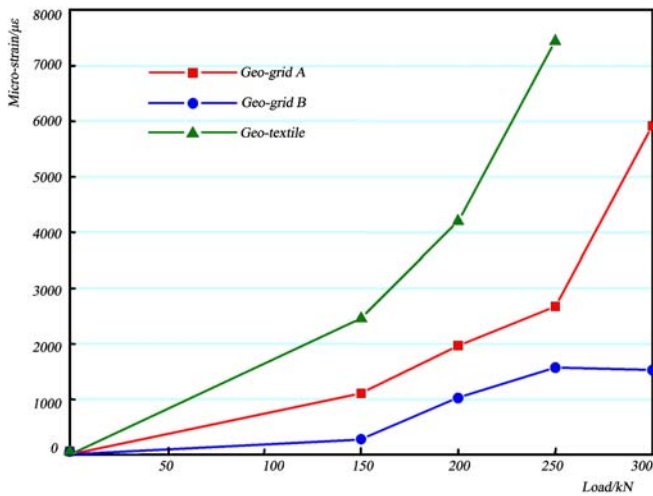


Fig. 8 Graphs of strain-load

buffer are very fragile. Nonuniform deformation and some hard particles (sand or gravel) will cause some partially large deformation along fibers and make the fibers broken. The result shows that the 250 μm without jacket buffer fiber is not suitable for monitoring the deformation of soil slope.

Figure 7 shows microstrains under different loads from other types of fiber sensors. The fiber sensors emplaced in the geotextiles are broken, and geotextiles are torn up at the pressure of 30 kN as is shown in Fig. 7a. The fiber sensors of Type C (JPEE jacket) are also partially broken at the pressure of 30 kN, as is shown in Fig. 7b.

As seen in Fig. 7, the strain attenuates from top to bottom, which fits the basic rule of stress delivering. However, the strain obtained from fiber sensor emplaced in geogrids (see Fig. 7c,d) that is just 10 cm beneath the fiber sensor emplaced in geotextiles (see Fig. 7a) attenuates greater. This shows that the geogrid is more effective in protecting the slope and reducing the deformation of the slope.

Before the slope failed, as the load increases, the strain increases very fast. When the slope failed, the increase of strain obtained from the geogrid B, which is beneath the geogrid A, is smaller than other fiber sensor parts. Figure 8 shows the increase of strain in V3 series taken from Fig. 7a,c, and e. The reason can be found by checking the failure surface of the failed slope by eyes. When the pressure is up to 300 kN, the geotextile is torn up and the soil mass slide along the surface of the geogrid A, which causes the stress decrease on the geogrid B.

The fiber Type C is planted directly in the soil, and different parts of the fiber sensors are nearly independent. Compared to the fiber sensor emplaced in geosynthetics, the strain that is far away from the loading plate is almost not affected by loading, but the strain that is just beneath the loading part is great as shown in Fig. 7b. On the contrary, if the soil deformation causes one part of the geosynthetics to move, other parts of the geosynthetics will also be pulled and the strain will be increased, as is shown in Fig. 7a,c,d,e, and f. This means that the strain obtained from fiber Type C can be better expressed by the soil strain than that from fiber sensors emplaced in geosynthetics. It is worth noting that the directions of the strains in different parts of the fiber sensors

are different, which cannot be identified just from the monitoring data in this test.

However, if the shear stress between the soil and the fiber surface are greater than their shear strength, the fiber would peel. Moreover, the measured strain with BOTDR is expressed as the averaged value over its spatial resolution (1 m in this test), and it is always smaller than the peak one. So, all of the fiber sensors described in this paper can only monitor averaged value rather than accurate soil strain. Moreover, all the microstrains obtained by BOTDR are one-dimensional strains along the fiber sensors rather than three-dimensional strain as it is being in soil slope. Nevertheless, the patterns of strain distribution can be found clearly. Figure 9 shows the nephogram of the maximum strain distribution before the slope failed. AS seen from Fig. 9a,c, and e, the greatest strain values of the V series are all in the medium sensor parts that are just beneath the loading part and attenuate from the loading place and far. For the H series, the greatest values are moved from the loading place to the place inside of the model (seen from Fig. 9b–f), which can also be found in Fig. 7b–f. This shows that the slope failure makes the strain distribution changed.

In fact, strain nephogram are more useful to express the abnormal strains distribution if the fiber sensors are used in large scale area monitoring rather than that of the small-scale test described in this paper.

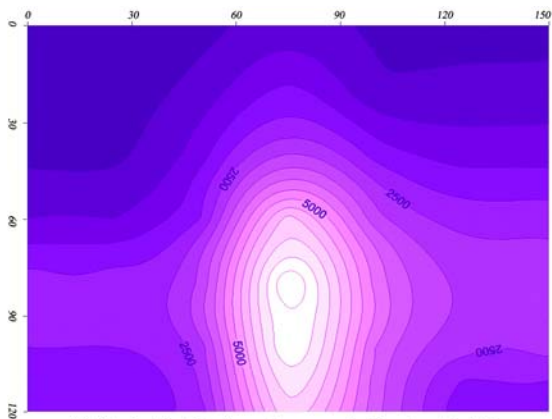
Conclusions and future works

Through the test and above analysis, it can be concluded that the application of distributed optic fiber monitoring to soil slope is more challenging than that to concrete structural object. The co-deformation between fiber sensors and the soil mass is the most essential issue. The achievement from this laboratory test can only prove that BOTDR technique is feasible to be used to monitor the abnormal deformation of soil slope, and also find some characteristics of strain distribution in soil mass and geosynthetics. Before BOTDR technique can be successfully applied to monitoring the stability of soil slope, more advanced test should be carried out in further study. Based on this laboratory test, some useful knowledge can be obtained as follows.

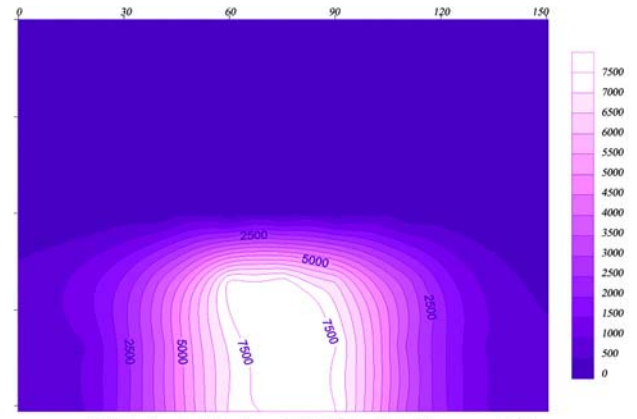
Because the fibers would be broken in the process of construction, the no-jacket-buffered fiber sensors cannot be directly planted into soil slope to monitor the deformation. Co-deformation of low-strength geotextile with nylon-jacket-buffered fiber and direct-planted TPEE jacket-buffered fiber is better than high-strength geogrid with nylon-jacket-buffered fiber, but the latter is fit for long-term monitoring because the fibers can keep undamaged even at relatively larger deformation.

Even though the limitation of the distance spatial of BOTDR technique, the rules of the strain distribution can also help us find and locate the abnormal strains. If appropriate layout of fiber sensors in artificial slope were designed, early-warning of the slope stability can be realized by analyzing the monitoring data obtained from BOTDR.

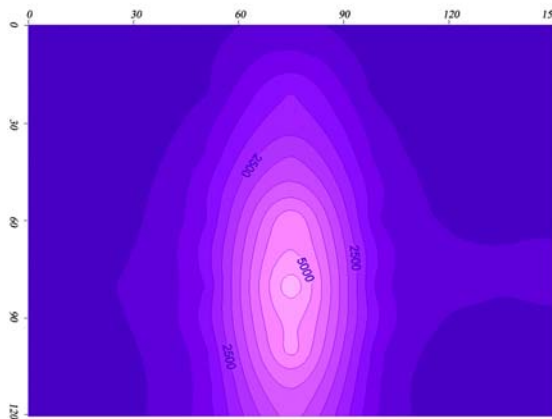
The test in this paper is carried out in a small scale model, the detail rules of the strain distribution cannot be clearly expressed, due to the limitation of distance resolution of BOTDR. In the future, some large-scale field test should be carried out for further research.



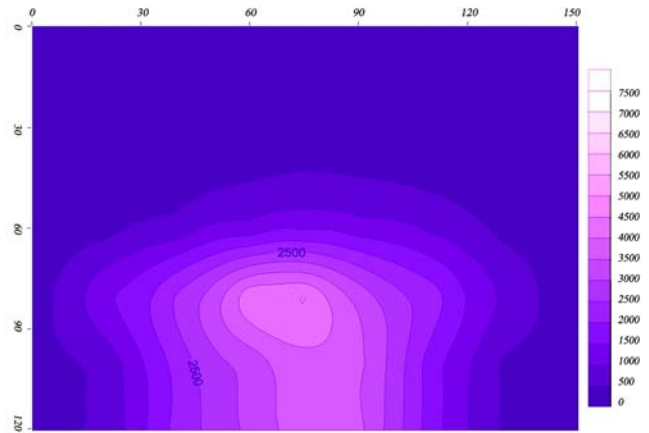
(a) Strain distribution of sensors in Geo-textile (V)



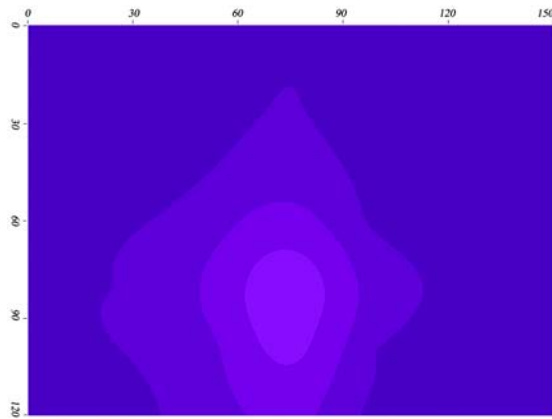
(b) Strain distribution of TPEE-buffered sensors (H)



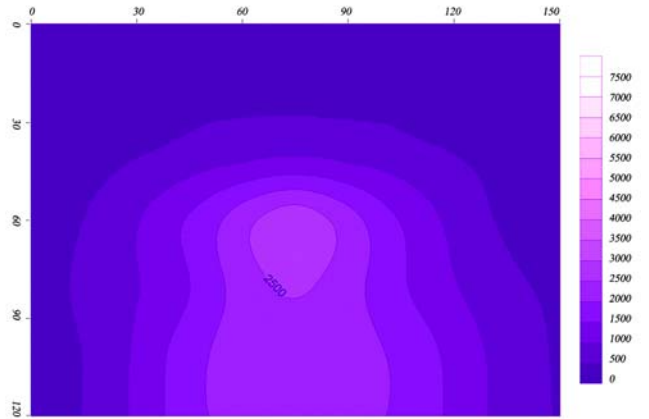
(c) Strain distribution of sensors in Geo-grid A (V)



(d) Strain distribution of sensors in Geo-grid A (H)



(e) Strain distribution of sensors in Geo-grid B (V)



(f) Strain distribution of sensors in Geo-grid B (H)

Fig. 9 Strain nephogram of different sensors

Acknowledgements

The authors gratefully acknowledge the financial support provided by National Natural Science Foundation of China (Grant No. 40572154)

References

Bao XY, Zhang CS, Li WH, Ozkan F, Mohareb M (2007) Using distribution Brillouin sensor to predict pipe deformation with carbon coated fibers. The Second International Workshop on Opto-electronic Sensor-based Monitoring in Geo-engineering. Nanjing, China, Oct.18–19 pp 9–19.

Bastianini F (2005) A Brillouin smart FRP material and a strain data post processing software for structural health monitoring through laboratory testing and field application on a highway bridge. SPIE 5765:600–611

Blatz JA, Bathurst RJ (2001) Behaviour of full-scale reinforced emankments loaded to failure by a strip footing near the crest. 54th Canadian geotechnical conference [C], Calgary, Alberta, 16–18 September, pp 481–489

Chang KT, Kim KT (2002) A study of slope movements using fibre optic distributed deformation sensor, KGS Fall National Conference pp 475–482

Christopher KYL, Niell E, Noah O (2000) A novel distributed optical crack sensor for concrete structures. Eng Fract Mech 65(2):133–148

Ding Y, Shi B, Cui HL, Gao JQ, Chen B (2003) The stability of optical fiber as strain sensor under invariable stress, proceedings of Structural Health Monitoring and Intelligent Infrastructure, Tokyo, Japan, November 13–15, pp 267–270.

Horiguchi T, Kurashima T, Tateda M (1989) Tensile strain dependence of Brillouin frequency shift in silica optical fibers. IEEE Photonics Technol, Lett 1(5):107–108

Lee KM, Manjunath VR (2000) Experimental and numerical studies of geosynthetic-reinforced sand slopes loaded with a footing. Can Geotech J 37 (4):828–842

Li AG, Yue ZQ, Tan GH (2003) Design and installation of comprehensive instrumentation system for slope in Hong Kong. Chinese J Geotechnical Eng 22(5):790–796 (in Chinese)

Ohno H, Naruse H, Kurashima T, Nobiki A, Uchiyama Y, Kusakabe Y (2002) Application of Brillouin scattering-based distributed optical fiber strain sensor to actual concrete piles. IEICE Trans Electron E85-C(4):945–951

Shi B, Sui HB, Zhang D (2007) Distributed monitoring of slope engineering. Second International Workshop on Opto-electronic Sensor-Based Monitoring In Geo-engineering, Nanjing, China, Oct.18–19, 81–86

Yin JH, Ding XL, Yang YW (2004) Intergration of conventional instruments and GPS for remote automatic monitoring of slopes. Chinese J Geotechnical Eng 23(3):357–364 (in Chinese)

Yoo C (2001) Laboratory investigation of bearing capacity behaviour of strip footing on geogrid-reinforced sand slope. Geotext Geomembr 19:279–298

Zhang D, Shi B, Xu HZ (2004) Experimental study on the deformation monitoring of reinforced concrete T-beam using BOTDR. J Southeast University, (Natural Science Edition) 34(4):480–484

B.-j. Wang (✉) · **K. Li** · **B. Shi** · **G.-q. Wei**

Center for Engineering Monitoring with Opto-Electronic Sensing, School of Earth Sciences and Engineering, Nanjing University, Hankou Road, 210093 Nanjing, People’s Republic of China
e-mail: baojun@nju.edu.cn